

## **OPTIMISING THE DESIGN OF GAS MICROSTRIP DETECTORS FOR SOFT X-RAY DETECTION**

J.E.Bateman, R. Barlow, G.E. Derbyshire, J.A. Mir and R. Stephenson

Rutherford Appleton Laboratory, Chilton, Didcot, Oxon, OX11 0QX, UK

10 January 2001

### **Abstract**

This report describes development work in which systematic changes in the electrode pattern of a Gas Microstrip Detector are explored in the search for higher avalanche gains and enhanced stability. It is found that the width of the cathode structure is the main determinant of the detector stability. With the correct cathode width, gas gains of  $>50\,000$  are comfortably attainable with low detector noise so that x-rays can potentially be detected down to the limit of a single x-ray-produced photoelectron.

## 1. Introduction

Introduced a decade ago, the gas microstrip detector (GMSD) [1] was developed intensively over many years for demanding applications in Particle Physics collider experiments. In particular the ability of the GMSD to function at very high counting rates with long lifetimes while delivering sub-millimeter spatial resolution was demonstrated. This work is fully documented in the reports of the RD-28 programme [2,3]. The recent proliferation of Synchrotron Radiation (SR) sources with their very intense x-ray beams has stimulated interest in the possibilities of applying this now mature technology in the field of materials studies using SR beams. Applications in x-ray diffraction studies [4,5] and Extended X-ray Absorption Fine Structure (EXAFS) [6,7] have been reported. Most of the work centres on the detection of x-rays in the energy region 5-10keV for which the gas gain ( $\approx 2000$ ) available from the standard GMSD design developed for Particle Physics applications is adequate. However, for sub-keV x-rays [7] the signal becomes marginal at such gains and a higher limiting gain is required. In surface EXAFS studies [8] it becomes necessary to use gas mixtures which do not give optimal gain conditions. In order to achieve adequate signals under such conditions, enhanced stability is required in the GMSD design.

This report describes development work in which systematic changes in the GMSD electrode pattern are explored in the search for higher avalanche gains and enhanced stability. It is found that the width of the cathode structure is the main determinant of the detector stability. With the correct cathode width, gas gains of  $>50\,000$  are comfortably attainable with low detector noise so that x-rays can be potentially detected down to the limit of a single x-ray-produced photoelectron.

## 2. GMSD Design and Operation

The GMSD patterns used in Particle Physics are geared towards maximum rate capability and high spatial resolution. A typical specification is: anode width 10 microns, cathode width 90 microns and pitch 300 microns. In a “good” gas mixture such as argon + 25% isobutane (or dimethylether) a maximum stable gain of up to 2000 can be achieved for a soft x-ray (for example Mn K at 5.9keV). When (for lower x-ray energies) helium is substituted for argon and a poorer quencher such as CO<sub>2</sub> is used, the maximum gain can drop to as low as 300, too low for comfortable operation. Studies at CERN showed that improved maximum gains of  $\approx 15\,000$  could be obtained by using wider cathodes [9,10] but with relatively limited scope for optimisation. In reference [11] it is shown that wider pitches permit gains high enough for the detection of photoelectrons, but the authors contest the view that the cathode width is the dominant element in stability at high gains.

In order to explore the gain/stability question a special GMSD plate was fabricated with the following specification. There are seven sections each containing twelve strip patterns of 0.5mm pitch with anodes of width 5 microns and the cathode width constant within a section but varying systematically between sections. All the anodes and cathodes of a section are connected together so that an active area of approximately 6mm x 18mm is formed which is connected to the standard charge amplifier sensing circuit. The cathodes of each section have the widths: 50, 90, 150, 200, 250, 300, 350 microns (sections #7, #6, #5, #4, #3, #2, #1). The patterns are

fabricated in 0.5 micron chromium on a 1mm thick plate of S8900 glass (50mm x 50mm). The plate is mounted in a gas-tight enclosure with a drift space of 10mm for x-ray conversion. For the tests reported, a gas mixture of argon + 25% isobutane is used throughout with a potential of  $-1400\text{V}$  applied to the drift electrode. The potential applied to the cathodes ( $V_c$ ) is negative with the anodes at earth.

The pitch of 500 microns was chosen because diffusion of the drifting electrons induces a spread of this order making it pointless to use a smaller pitch in an x-ray detector with a useful drift distance. The anode width was chosen in the light of earlier results which showed that this value represents the optimum for gas gain in a GMSD structure [12].

### 3. Gain Measurements

The gas gain of each section was measured in the usual way by comparing the peak of the pulse height distribution generated by Mn K x-rays with a charge calibrator. An energy per ion pair of  $27\text{eV}$  was assumed for the gas mixture. Figure 1 shows the set of gain versus  $V_c$  curves obtained from the seven sections. The maximum gain point in each set corresponds roughly to the maximum stable operating point in each case. Figure 2 shows two typical pulse height spectra at medium ( $M=3553$ ) and high ( $M=45\,562$ ) gains for section #3 (the amplifier gains are adjusted to bring the peaks together). Figure 3 summarises the limiting gain parameters of the seven sections with the maximum gain ( $M_{\text{max}}$ ) rising as the cathode width increases and the  $V_{\text{cmax}}$  falling. As Figure 2 shows, the only detectable difference between a pulse height spectrum taken at maximum gain and one taken at medium gain is a slight increase in the energy resolution. Figure 4 shows a plot of the energy resolution (relative FWHM) as a function of the gain for section #1. This is the typical response of a GMSD with an optimum resolution of  $\approx 14\%$  for Mn K x-rays at medium gas gain ( $500 < M < 3000$ ) with a slight deterioration at the highest gains. The energy resolution of all sections behaves in a similar manner with a  $\text{FWHM} \approx 20\%$  at  $M = M_{\text{max}}$ .

### 4. Noise Measurements

Addressing the problem of detecting very low energy ( $< 1\text{keV}$ ) x-rays, the key requirement is a low noise threshold as measured in terms of the energy deposit in the detector. This is quantified by defining a Noise Floor Energy ( $E_{\text{NF}}$ ) such that the total noise counting rate above a threshold set at this energy is  $10\text{Hz}$ . This rate is defined arbitrarily as well in excess of the cosmic ray background ( $\approx 0.01\text{Hz}$ ), but, since the rise of the noise counting rate is extremely steep, large changes in the chosen rate cause little change to  $E_{\text{NF}}$ . The calibration of the energy scale was made by using the Mn K lines and their argon escape peaks. Since the typical values of  $E_{\text{NF}}$  are  $< \approx 100\text{eV}$  and the lines are at  $3000\text{eV}$  and  $6000\text{eV}$  considerable extrapolation is required. It was found that provided the pulse height peaks were assigned the weighted energies of the Mn  $K_\alpha$  and  $K_\beta$  lines (which are not resolved by the detector) extrapolated  $E_{\text{NF}}$  values could be calibrated down to  $\approx 10\text{eV}$  with errors generally  $< 10\%$  in  $E_{\text{NF}}$ .

Figure 5 shows  $E_{\text{NF}}$  plotted as a function of  $V_c$  for the detector sections. As expected the noise floor decreases with increasing  $V_c$  (i.e. gas gain). In the case of high gain

sections (#1, #2, #3)  $E_{NF}$  reaches 10eV or below, implying that single photoelectrons are potentially detectable. Two sections, (#2 and #5) show anomalous increases in the noise floor at the highest gains. Figure 6 summarises the minimum noise floor  $E_{NFmin}$  achieved by each section. The smooth line is a fit to the five “well-behaved” sections and shows a systematic improvement in the noise floor with the cathode width with the two “noisy” sections sitting well above the fitted curve.

A second measure of the system noise is available in the width of the charge calibration pulse height distribution. With  $V_c=0$  this is just the amplifier noise which is expected to be dominated by the series noise generated by the section electrode capacitance and resistance combined with the corresponding parameters of the FET input of the preamplifier. Measurement shows that a typical section looks like a parallel capacitor of 16pF with a series resistance of 600 ohms. Figure 7 shows the measured pulser noise width and capacitance for each section. The variation of the noise with cathode width is small (<10%) with a typical value of  $\approx 1200$  electrons (standard deviation). For smaller cathode widths it seems to be proportional to the capacitance as expected from the series noise term. The effect tending to reduce the noise at the highest cathode widths has not been identified. The pulser noise shows no detectable variation with the  $V_c$  (i.e. gas gain) for any section.

## 5. Discussion

### Gain Stability

It is clear from figure 3 that the general behaviour of  $M_{max}$  as a function of the cathode width is very similar indeed to that predicted by the model of reference [9] (figure 17). When the CERN group tested a detector with variable cathode widths ( $d_C$ ) and a fixed 200 micron pitch ( $d_P$ ) the results did not confirm their model and only a modest increase in  $M_{max}$  ( $\approx 15\ 000$ ) was obtained with  $d_C = 90$  microns and a decrease for wider cathodes [10]. The present results with  $d_P = 500$  microns give a maximum  $M_{max}$  ( $\approx 55\ 000$ ) at  $d_C = 300$  microns. These results can be interpreted in terms of the electric field pattern around the cathode (see reference [9] figure 14).

The field around the cathode is characterised by relatively uniform field strength over most of the width with cusps at the edges with a FWHM of  $\approx 5$  microns. As  $d_C$  increases the mean field over the cathode decreases and the anode and cathode cusp fields increase for a given  $V_c$ . The increase in the anode field means that a given gain is attained at a lower  $V_c$  (figure 3) decreasing the cathode fields appropriately. Because of its narrow spatial extent the cathode cusp field is inefficient at generating gain from electrons leaving the cathode edge which could potentially initiate a noise pulse or spark. However, as the anode-cathode gap ( $d_G$ ) narrows this process will become inevitable. One may, therefore anticipate that there is a limit to how small  $d_G$  may be made, which will depend on such variables as the gas composition, the cathode material, the quality of the etching along the edges and the substrate material. The maximal gain value for  $d_G$  in the set-up of reference [10] is 51.5 microns and in the present results is 97.5 microns. In their case the gas mixture (argon + 50% DME) is stronger (i.e. more UV absorbent) than argon + 25% isobutane and the metallisation (gold) is generally found to be more stable than chromium. This may account for the difference.

It would appear that the larger pitch of the present design allows the principle of the model in reference [9] to be exploited more fully before reaching the limit set by the minimum of the anode-cathode gap. Tests of the present design with stronger gas mixtures should show further increases in  $M_{\max}$  with a lower permissible  $d_G$ .

In the model of reference [9] diffusion of electrons travelling from the cathode edge to the anode is neglected. In a drift of 100 microns in these very high fields, electrons will random walk transversely by distances of the order of tens of microns in any gas [13]. On the scale of the detectors under study this means that very few electrons will actually follow one of the very high gain paths studied in reference [9]. They will either hit the substrate and be absorbed or move out into regions of lower field strength (and thus lower gain). This is probably a stabilising factor against edge breakdown.

### Noise

In the absence of noise generated by the detector, the noise floor energy is expected to be proportional to the white (electronic) noise divided by the avalanche gain. Figure 8 shows that for section #1 this is approximately true. A fit of  $E_{NF}$  to the function  $a/M$  over the four lowest gain values is excellent with the measured values drifting slightly above the fit at the highest gains. Expressed in terms of the standard deviation ( $\sigma_e$ ) of the pulser pulse height distribution  $a = 5.4\sigma_e$  or  $2.29FWHM_e$ . This confirms the general rule-of-thumb that the useful noise floor in a system dominated by white noise is just twice the FWHM of the pulser spectrum. In the most general terms:

$$E_{NF} = \frac{5.4w\sigma_e}{M} \quad (1)$$

where  $w$  is the energy per ion pair of the gas mixture. Equation (1) describes the noise floor energy of sections #1, #3, #4 and #7.

Figure 8 shows how the noise floor energy of section 2 departs from this functional dependence at gains above 10 000. Figure 9 shows the noise pulse height distributions obtained from section #2 in this region. Below the critical value of  $V_c$  the noise distribution is just the gaussian of the white noise but as  $V_c$  increases two broadly peaked pulse distributions appear. At maximum gain ( $V_c = 740V$ ) the peak of the strongest distribution occurs at a charge value of  $\approx 12\ 000$  electrons. Plotting the "gain" of this peak against  $V_c$  shows that it increases more slowly than the gain curve for the x-ray signal. The implication of these observations is that the source of the electrons which are being amplified lies close to the anode so that the full amplification available from the drift region is not experienced. This would implicate a processing imperfection in the anode-cathode gap on the surface as the source of the excess noise signals. The behaviour of section #5 is similar and the noise characteristics of both the good and bad sections were stable and repeatable, tending to confirm structural defects as the source of the excess noise.

## 6. Conclusions

It has been shown that the maximum stable gain of a GMSD can be increased by a factor of  $\approx 20$  by increasing the relative width of the cathode strips. If a pitch of 500 microns is selected, the increase of the maximum stable gain with the cathode width is seen to follow the general predictions of the model in reference [9]. The limit to the increase available by this method is probably set by a combination of the properties of the counter gas, detector substrate and metallisation. It is believed that with further attention to these details gas gains in excess of 100 000 can be achieved. No significant degradation in the energy resolution accompanies high gain operation.

For application to the detection of sub-keV x-rays it is important that this gain is achieved without the onset of gas-mediated noise processes. In the present case gains of  $\approx 55\,000$  can be achieved with essentially only the electronic white noise present, giving useful noise floor energy of  $< 10\text{eV}$  and potentially permitting the detection of single photoelectrons. This performance depends, however, on a high degree of perfection in the lithography on the plate. Two sections out of the seven on the plate showed repeatable noise sources which considerably degraded the noise floor energy. However, even with these faults the “bad” sections are potentially useful for the detection of sub-keV x-rays.

## Acknowledgement

The GMSD plates were manufactured by Baumer IMT, Greinfensee, Switzerland.

## References

1. A. Oed, Nucl. Instr. and Methods **A263** (1988) 351
2. F. Sauli, RD-28 Status Report: Development of gas microstrip chambers for radiation detection and tracking at high rates, CERN/DRDC/93-34 (1993)
3. F. Sauli, Development of gas microstrip chambers for radiation detection and tracking at high rates, CERN/DRDC/94-45 (1995)
4. V. Zhukov, F. Udo, O. Marchena, F.G. Hartjes, F.D. van der Berg, W. Bras, E. Vlieg, Nucl. Instr. and Methods **A392** (1997) 83
5. J.E. Bateman, J.F. Connolly, G.E. Derbyshire, D.M. Duxbury, J. Lipp, J.A. Mir, R. Stephenson, J.E. Simmons and E.J. Spill, B.R.Dobson, R.C.Farrow, W. I. Helsby, R. Mutikainen and I. Suni, A Gas Microstrip Wide Angle X-ray Detector for Application in Synchrotron Radiation Experiments, Presented at the 5<sup>th</sup> International Conference on Position Sensitive Detectors, University College, London, 13-17 September 1999, to be published in Nucl. Instr. and Methods
6. A.D. Smith, J.E. Bateman, G.E. Derbyshire, D.M. Duxbury, J.D. Lipp, E.J. Spill and R. Stephenson, A gas microstrip x-ray detector for soft energy fluorescent EXAFS, presented at SRI 2000, to be published in Nucl. Instr. and Method.

7. J.E. Bateman, G.E. Derbyshire, E. Dudzik, G. van der Laan, J.D. Lipp, A.D. Smith and R. Stephenson, A new x-ray detector for magnetic circular dichroism experiments, presented at SRI 2000, to be published in Nucl. Instr. and Method; also J.E. Bateman, G.E. Derbyshire, E. Dudzik, G. van der Laan, J.D. Lipp, A.D. Smith and R. Stephenson, A gas microstrip x-ray detector for application in magnetic circular dichroism experiments, RAL-TR-2000-041 (<http://www-dienst.rl.ac.uk/library/2000/tr/raltr-2000041.pdf>)
8. T. Rayment, S.L.M. Schroeder, R.M. Lambert, G.D. Moggridge, J.E. Bateman, G.E. Derbyshire and R. Stephenson, "Auger electron detection at ambient pressures for x-ray absorption spectroscopy", unpublished.
9. T. Beckers, R. Bouclier, Ch. Garabatos, G. Million, F. Sauli and L.I. Shekhtman, Nucl. Instr. and Method **A346** (1994) 95
10. R. Bouclier, M. Capeans, C. Garabatos, G. Manzin, G. Million, L. Ropelewski, F. Sauli, T. Temmel, L. Shekhtman, V. Nagaslaev, Yu. Pestov and A. Kuleshov, Nucl. Instr. and Method **A365** (1995) 65
11. V. Peskov, B.D. Ramsey and P. Fonte, Nucl. Instr. and Method **A392** (1997) 89
12. J.E. Bateman, J.F. Connolly, G.E. Derbyshire, D.M. Duxbury, J. Lipp, J.A. Mir, R. Stephenson, J.E. Simmons and E.J. Spill, Studies of the gain properties of Gas Microstrip Detectors relevant to their application as X-ray detectors, Rutherford Appleton Laboratory Report, RAL-TR-1999-057, (<http://www-dienst.rl.ac.uk/library/1999/tr/raltr-1999057.pdf>) Presented at the International Workshop on Micro-Pattern Gas Detectors, Orsay, France, 28-30 June 1999.
13. A. Peisert and F. Sauli, Drift and diffusion of electrons in gases: a compilation, CERN/84-08/1984

### Figure Captions

1. Avalanche Gain versus  $V_c$  curves for the seven sections of the test detector. The lines are model fits. The gas is argon + 25% isobutane and the drift electrode potential is  $-1400V$ .
2. Typical pulse height analyser spectra obtained with Mn K x-rays ( $^{55}Fe$  source) in a section of the detector at medium ( $M=3553$ ) and high ( $M=45562$ ) gains. The amplifier gain is adjusted to bring the peaks together.
3. The maximum stable gain achieved by each section ( $M_{max}$ ) and the corresponding anode-cathode potential ( $V_c$ ) as a function of the cathode width of the section.
4. The relative energy resolution (FWHM) of the Mn K x-ray lines as a function of the gas gain in a high gain section (#1).
5. The noise floor energy ( $E_{NF}$ ) as a function of  $V_c$  for the detector sections.

6. The minimum noise floor energies from figure 5 plotted as a function of the cathode width of the section. The line is a ln-ln fit to the four “good” sections.
7. The electronic pulser noise width (standard deviation) and the measured section capacitances plotted as a function of the section cathode width.
8. The noise floor energy plotted for sections #1 and #2 as a function of the gas gain along with a fit to the lowest four gain points of the form  $N_{EF} = \text{constant}/M$ .
9. The pulse height spectra of the noise pulses observed in section #2 at higher gain settings.

FIGURE 1

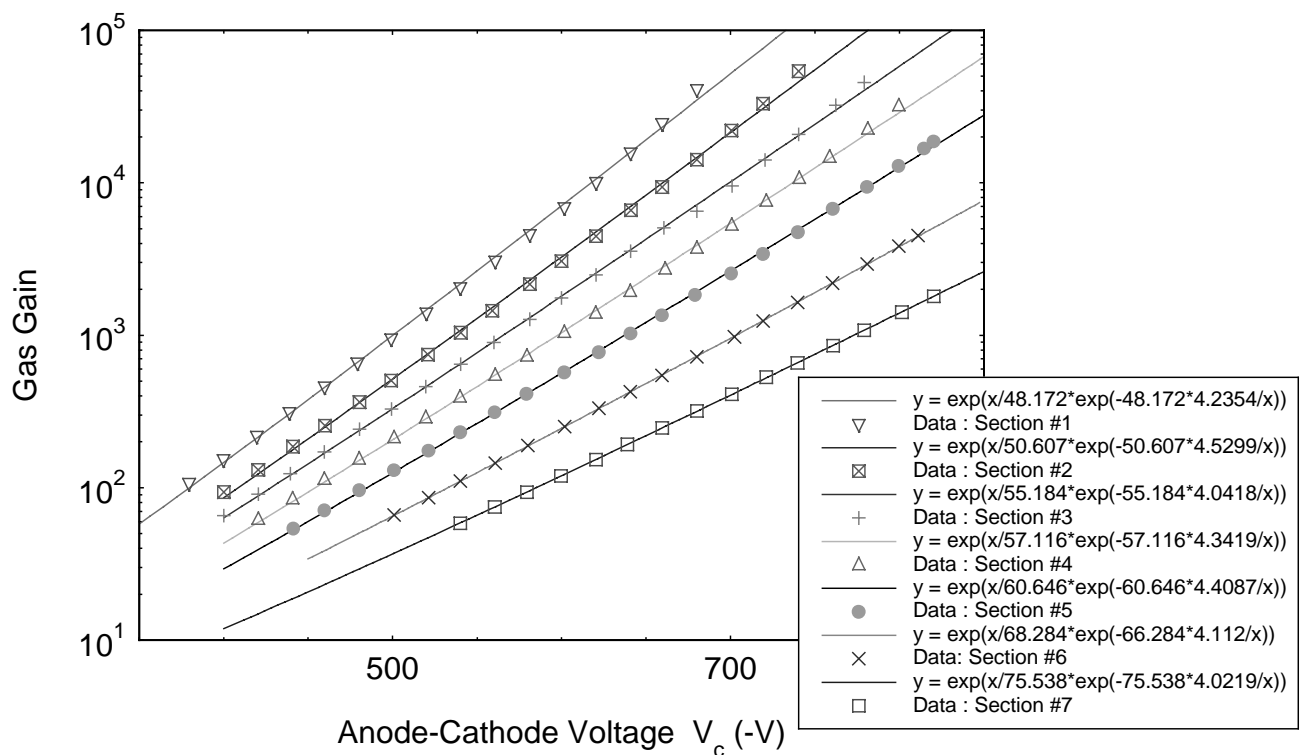




FIGURE 2

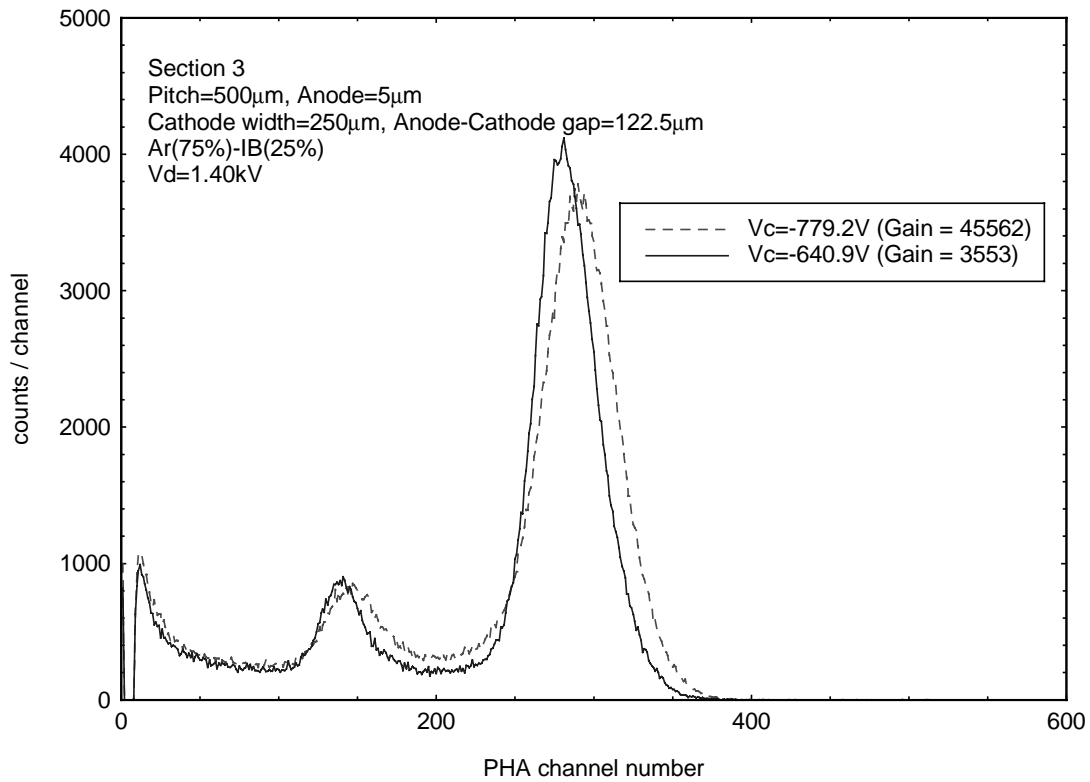


FIGURE 3

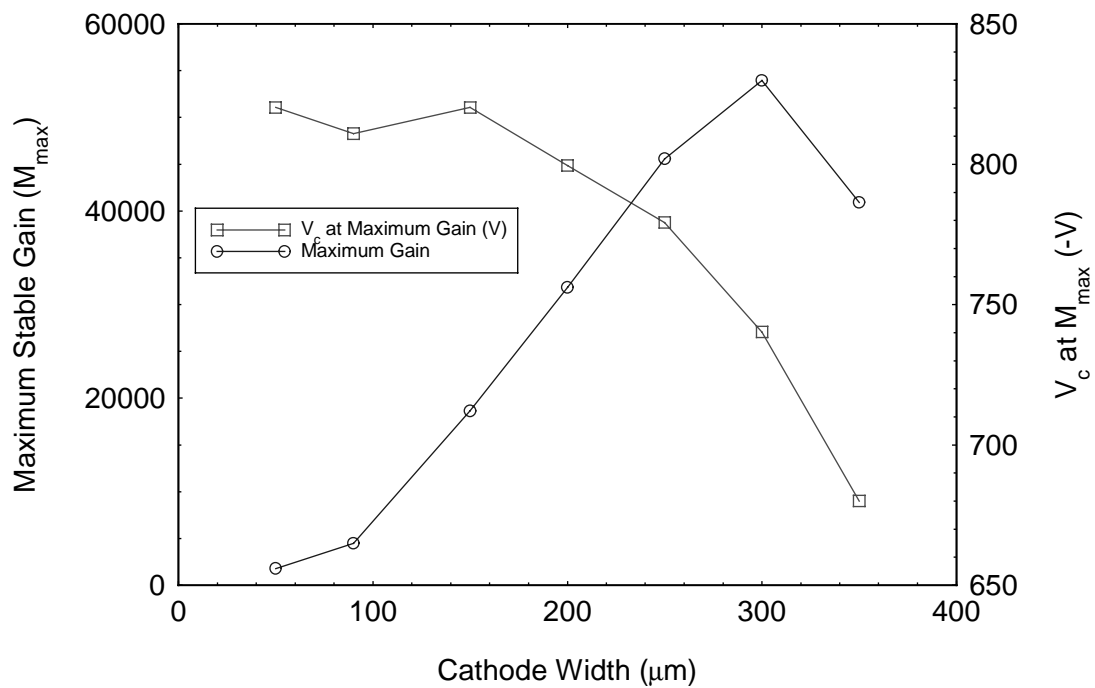


FIGURE 4

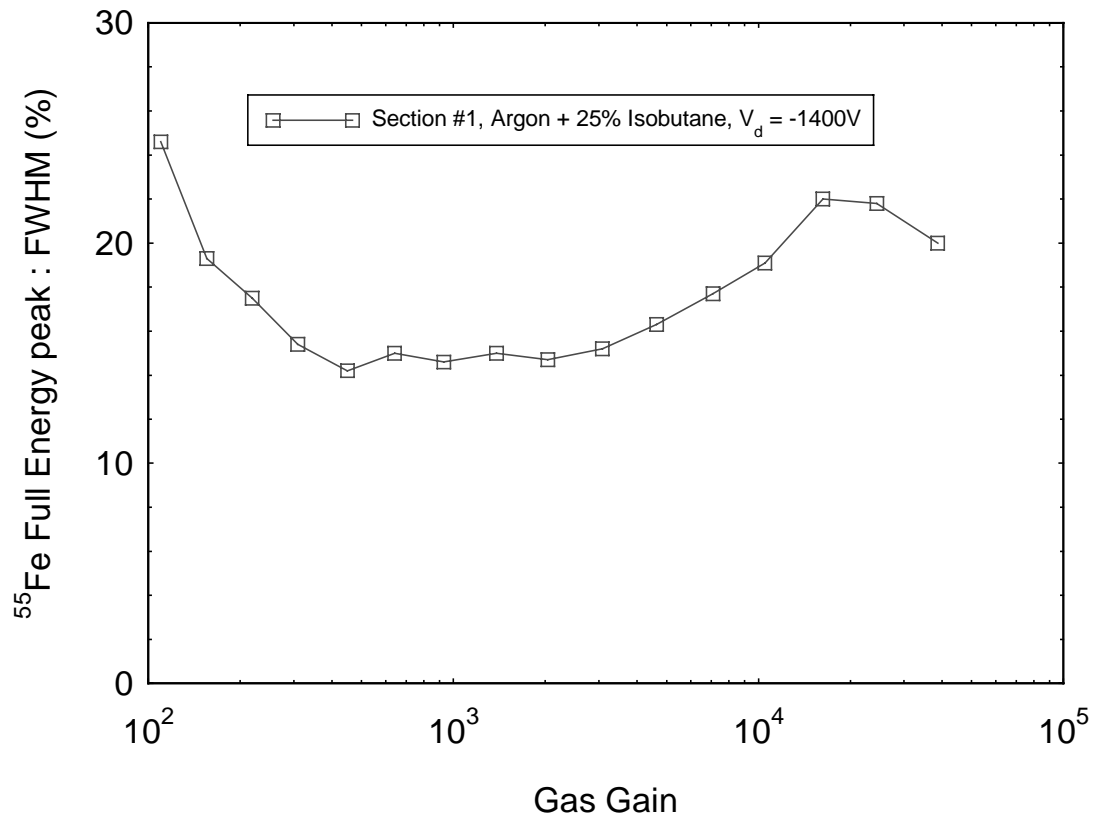


FIGURE 5

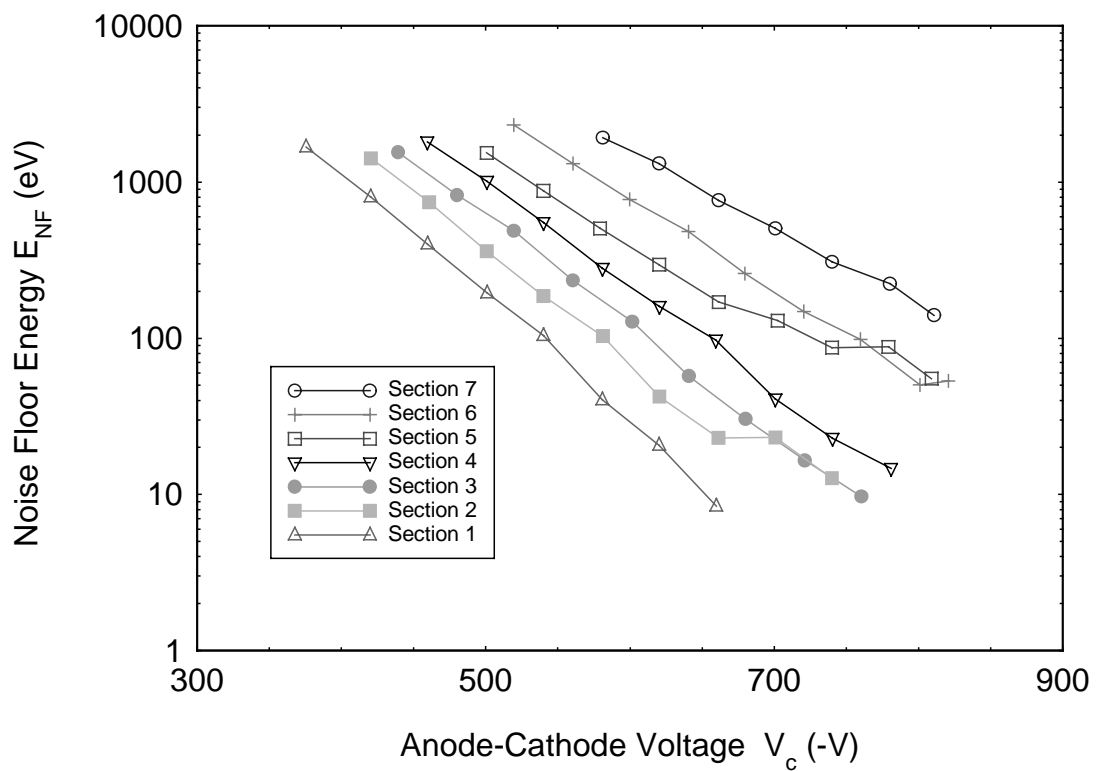


FIGURE 6

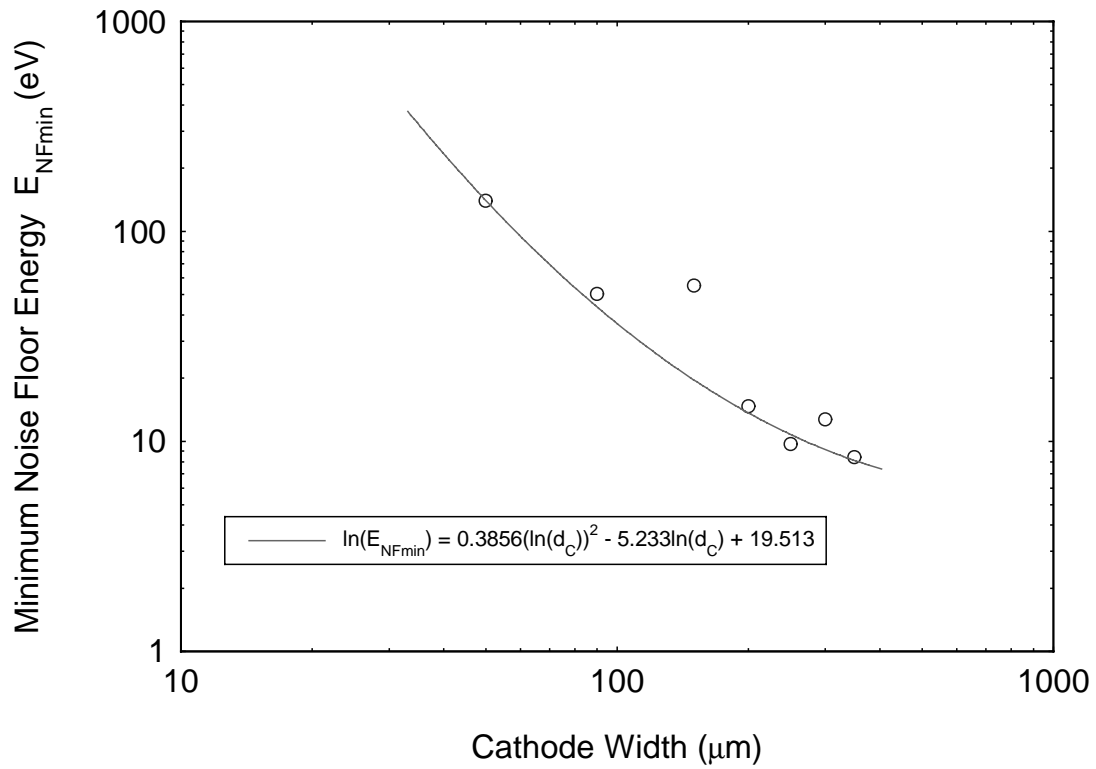


FIGURE 7

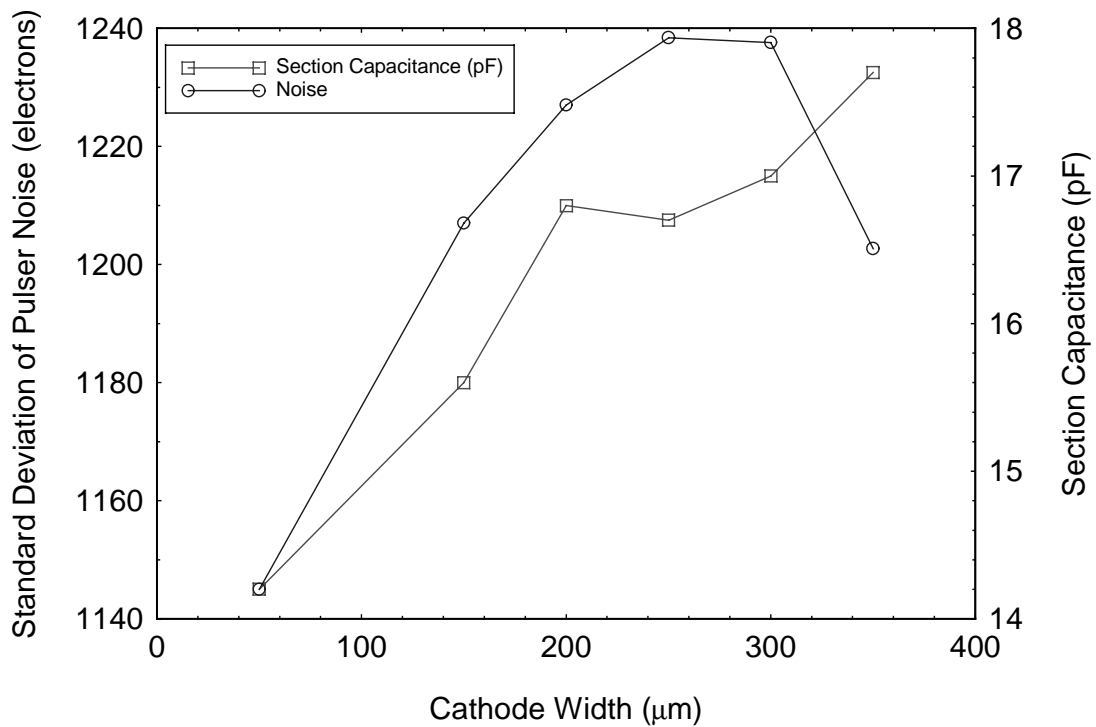


FIGURE 8

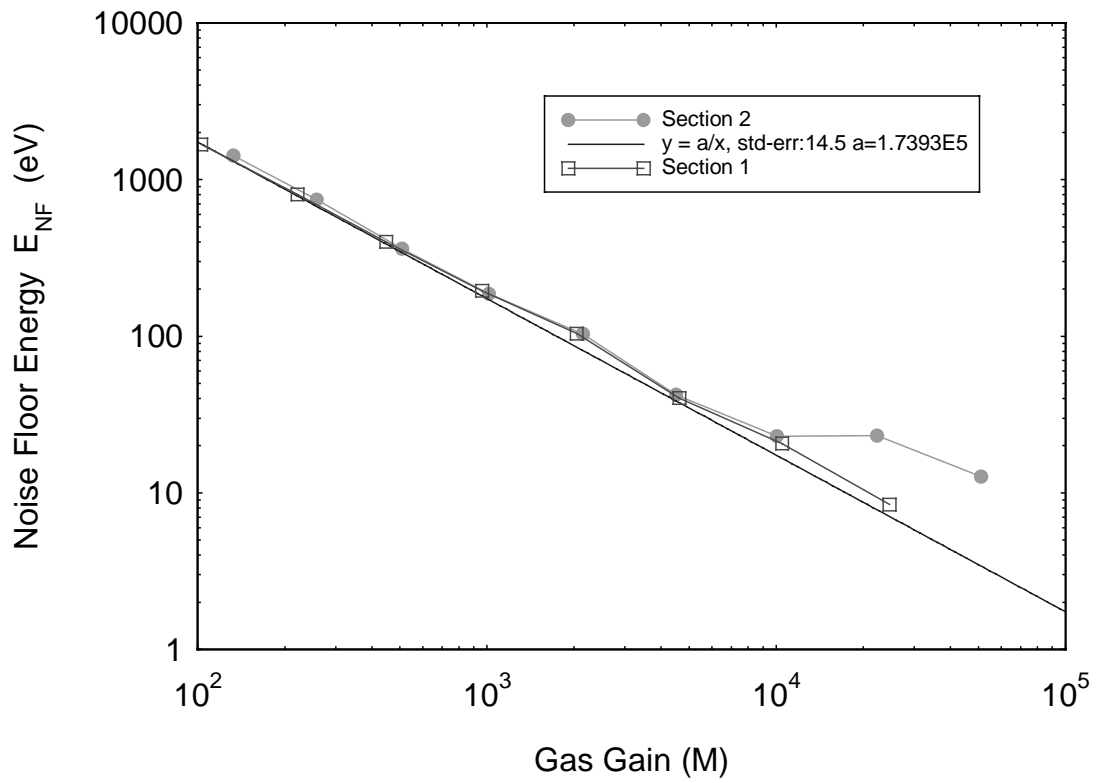


FIGURE 9

